Biosensors and Bioelectronics 126 (2019) 30–35

Contents lists available at ScienceDirect

Biosensors and Bioelectronics

journal homepage: www.elsevier.com/locate/bios

Organic molecular passivation of phosphorene: An aptamer-based biosensing platform

Shan Liang[a], Lidong Wu[b,*], Huan Liu[b], Jincheng Li[b], Mengze Chen[c], Min Zhang[a]

[a] Beijing Advanced Innovation Center for Food Nutrition and Human Health, Beijing Technology and Business University, Beijing 100048, China
[b] Key Laboratory of Control of Quality and Safety for Aquatic Products, Ministry of Agriculture, Chinese Academy of Fishery Sciences, Beijing 100141, China
[c] Food Science and Engineering College, Beijing University of Agriculture, Beijing 102206, China

ARTICLE INFO

Keywords:
Passivation of phosphorene
PP-AuNP nanocomposite
Aptamer
Electrochemistry
Biosensor

ABSTRACT

Black phosphorus (BP), also known as phosphorene (PP), is a fascinating two-dimensional (2D) material with extraordinary anisotropic mechanical, electronic and optoelectronic properties. However, PP is sensitive to oxygen and moisture and is completely degenerated by oxygen and humid air within 12 h, which limits its applications. Here, we coat PP with hexamethylenediamine (HMA), which allows the coated PP to maintain its original form in aqueous solution for over one month. The stable PP is dotted with gold nanoparticles to facilitate binding to a 3,3′4,4′-polychlorinated biphenyl (PCB77) aptamer (ap) as a biosensor. The aptamer biosensor based on gold nanoparticle-dotted PP nanocomposites (PP-AuNPs) exhibits superior analytical performance, and its sensitivity (391.1 μA cm^{-2}) is approximately three times higher than that of an AuNP-based sensor (AuNP-Ap/Au electrode, 147.2 μA cm^{-2}). This biosensor has a low detection limit (DL) of 33 pg L^{-1} toward PCB77 with a dynamic response range toward PCB77 from 100 pg L^{-1} to 10 μg L^{-1}. This research opens up avenues for the use of PP to make multiplexed diagnosis platforms in aqueous systems.

1. Introduction

Single-layer or few-layer black phosphorus (BP), also known as phosphorene (PP), was successfully isolated in 2014 and has attracted high research interest due to its extraordinary properties (Bui and Yarmohammadi, 2018; Guo et al., 2018; Li et al., 2014a). Monolayer BP is a new two-dimensional (2D) material with high carrier mobility (ca. 1000 $cm^2/V\,s$, along the armchair direction)(Li et al., 2014b; Qiao et al., 2014) in which each phosphorus atom is bonded with three adjacent phosphorus atoms to form a puckered honeycomb lattice (Jiang and Park, 2014a,b). However, PP is highly sensitive to oxygen and humidity due to the two lone pairs of electrons in each phosphorus atom (caused by sp^3 hybridization) and its enormously high surface to volume ratio (Mayorga-Martinez et al., 2015). This issue leads to significant deterioration in device performance in humid conditions (Lee et al., 2017; Li et al., 2017; Miao et al., 2017).

Several approaches have already been applied to improve the stability of PP (Hu et al., 2018; Zhang et al., 2018). The main strategies in passivation of PP are encapsulating PP by oxidizing the top layer of phosphorene by oxygen plasma dry etching (Wan et al., 2018), capping PP with 2D graphene (Xing et al., 2017), and covalent functionalization and non-covalent functionalization. They are all recent efforts to ameliorate its problematic air and moisture instability (Jeong et al., 2018; Late, 2016). However, plasma etching and covalent functionalization inevitably introduce undesirable and irreversible detects to PP, and capping 2D graphene layer against degradation introduce unwanted source of surface. Non-covalent functionalization can keep the intrinsic property of PP and serve as a physical barrier preventing oxygen from reaching the surface. Nowadays, the PP obtained by the solvent exfoliation method is still sensitive to humid air (Late, 2016). Here, we passivate PP with self-assembled monolayers of hexamethylenediamine (HMA) in chloroform to eliminate its instability under oxygen and humid conditions. The HMA coating PP not only keep PP's originally puckered honeycomb structure and thus good conductivity, but also enhance PP's stability and dispersion in aqueous solution. The HMA coating on the surface of the PP enables the PP to maintain its original form in aqueous solution over one month.

This stable PP with high electrical conductivity and a large surface area has attracted increasing attention, and more researchers will use PP as a multiplexed diagnosis platform in aqueous system. As is well known, the use of 2D materials has been established in the sensitive detection of biomolecules and environmental pollutants (Wu et al., 2012). Superior biosensing materials are the core technology for improving the long-term stability of biosensors in vitro, their detection

* Corresponding author.
E-mail address: lidongwu@mit.edu (L. Wu).

https://doi.org/10.1016/j.bios.2018.10.037
Received 3 September 2018; Received in revised form 16 October 2018; Accepted 18 October 2018
Available online 21 October 2018
0956-5663/

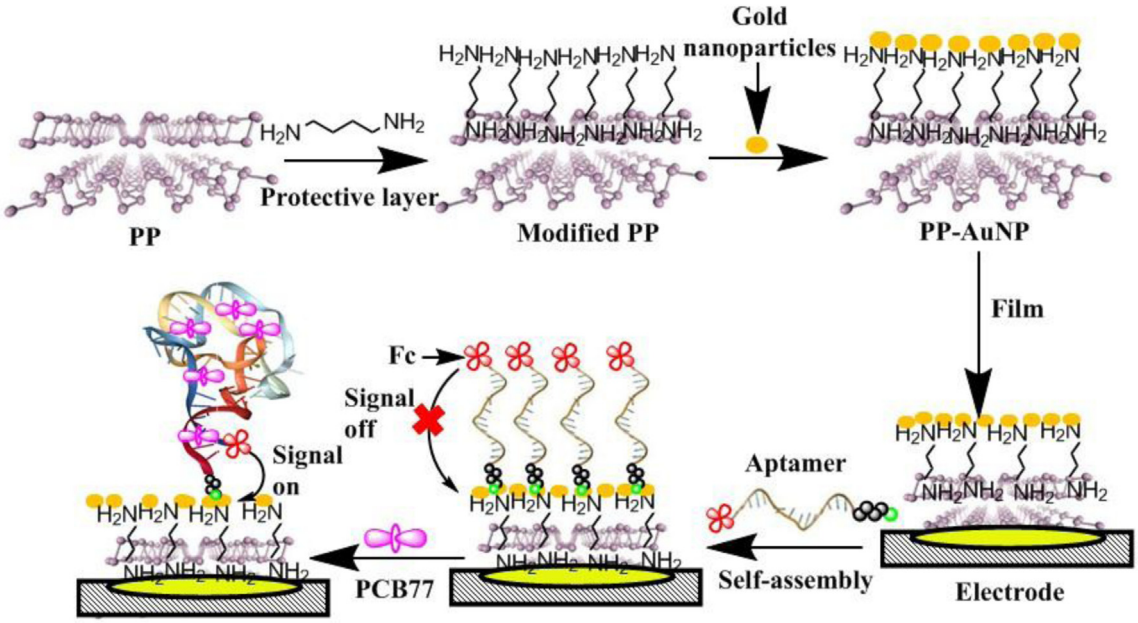

Scheme 1. Schematic diagram of the fabrication process and detection mechanism of the PP-AuNP-Ap/Au biosensor. The PP is placed in chloroform with HMA, and then gold nanoparticles are anchored on the surface of the PP. The PP-AuNP nanocomposites are immobilized on the Au electrode, and then thiolated aptamer solution is dropped onto the PP-AuNP-modified Au electrode. The fabricated PP-AuNP-aptamer biosensor is used for the detection of PCB77. The green ball is the thiol group on the end of the aptamer.

limit (DL) and sensitivity, etc. Liu et al. have compounded PP with Co_3O_4 and TiO_2 to improve the electrochemical performances (Liu et al., 2018; Luo et al., 2018; Tan et al., 2017). In this work, PP has been dotted with gold nanoparticles (AuNPs) that function as binding sites to anchor additional biomolecules on the underlying PP. The combination of the aptamers with nanomaterials is promising in the development of biosensing platform (Kumar et al., 2016; Zhao et al., 2018). Thiol-modified DNA aptamers for 3,3′4,4′-polychlorinated biphenyl (PCB77) are isolated from a pool of random-sequence oligonucleotides using the systematic evolution of ligands by exponential enrichment (SELEX) method.(Xu et al., 2012) The aptamer is immobilized on the stable PP-AuNPs via self-assembly interactions between the AuNPs and aptamers. The prepared biosensor displays high sensitivity and specificity for PCB77 and is a promising candidate for the rapid determining PCB77 on site.

2. Experimental section

2.1. Materials and solutions

3,3′4,4′-PCB (PCB77), 3,4,4′,5-PCB (PCB81), 3,3′,4,4′,5-PCB (PCB126) and 2,3,3′4,4′5,5′-PCB (PCB189) are obtained from Dr. Ehrenstorfer (Germany). HMA, chloroform, hexachlorobenzene (HCB), and other chemicals are purchased from Sigma-Aldrich (USA). The aptamer sequence is 5′-SH-$(CH_2)_6$-GGCGGGGCTACGAAGTAGTGATTT TTTCCGATGGCCCGTG-Fc-3′ which is synthesized through Takara Biotechnology Co. Ltd. (Dalian, China). The aptamer is stored in 20 mmol L^{-1} pH 8.0 Tris-HCl.

2.2. Apparatus

Transmission electron microscopy (TEM) images are obtained by a JEM-2100 (Japan). Scan electron microscopy (SEM) images are obtained by a Zeiss Sigma 300 (Germany). Atomic force microscopy (AFM) is performed using peak force mode and a silicon nitride cantilever tip (Bruker, USA). Raman samples are prepared by dropping PP suspension on SiO_2 substrate and recorded using raman spectra (Thermo, USA). X-ray Diffraction (XRD) patterns are recorded by an X-ray diffractometer (Bruker, Germany). A CHI 660B Electrochemical Workstation (CHI Instruments Inc.) works for cyclic voltammetry (CV) and differential pulse voltammetry (DPV). The three-electrode system is an Au electrode as the working electrode, an Ag/AgCl electrode as the reference electrode, and a platinum wire as the auxiliary electrode.

2.3. Preparation of PP and PP-AuNPs

The PP preparation process divides into two steps and performed in an acrylic glove box to maintain specified levels of H_2O and O_2, which are necessary for the uniform oxidation and hydroxylation of the PP surface layer. First, the BP materials are exfoliated by ultrasonication in chloroform and DMF (1:1) with an argon supply to remove dissolved oxygen molecules. The supernatant contains the PP and is collected after centrifugation to remove the unexfoliated particles. The PP is transferred onto a SiO_2/Si wafer and immersed in a glass vial, which is capped and placed inside silicone oil. The silicon oil is then heated to 130 °C and maintained for 20 min. After this step, the –OH groups form on the surface of the PP. Then, the PP is transferred into chloroform with HMA at 100 °C for 30 min to allow the HMA molecules to link to the PP surface through proton transfer from -OH to -NH_2, thus forming ionic bonds. As a result, a more continuous and uniform protective monolayer is formed on the surface of the PP.

Gold nanoparticle-dotted PP nanocomposites (PP-AuNP) are prepared by the seed-induced growth method. First, 50 mL of 0.1 mg mL^{-1} chloroauric acid and 50 mL of 0.25 mg mL^{-1} PP solution are mixed together for 10 min, and then added 2.5 mL 4 mg mL^{-1} vitamin C in the above solution. Finally, 0.5 mL 10 mg mL^{-1} sodium citrate is used for stopping the chemical reaction. After centrifugation at 1300*g* for 5 min three times, the PP-AuNP nanocomposite is obtained.

2.4. The PP-AuNP-Ap/Au electrode constructed process

To obtain a clean electrode, the Au electrode surface is cleaned by 0.05 μm diameter alumina powder and then ultrasonically washed with deionized water and ethanol three times each. Subsequently, the Au electrode is electrochemically cleaned by potential scanning in 1 mol L^{-1} H_2SO_4 from 0 to 1.7 V until reproducible CV are obtained. The

biosensor preparation process is shown in Scheme 1: the solution of PP-AuNPs (0.5 mg mL^{-1}) is shaken through ultrasound for 30 min. Subsequently, the droplet containing materials is added to the surface of the electrode. And the thiolated aptamer solution (8 μL, 1 μmol L^{-1}) is added on the surface of PP-AuNP-anchored Au electrode for 2 h at 25 °C. Finally, the PP-AuNP-Ap/Au biosensor is obtained.

Excess deionized water is used for washing all of the electrodes to remove weakly adsorbed aptamers before electrochemical measurements. The preparation protocols for the other electrodes are similar to that of the PP-AuNP-Ap/Au electrode. The PP-AuNP-Ap/Au electrode and other electrodes are characterized by electrochemical scanning in 5 mmol L^{-1} $[Fe(CN)_6]^{4-/3-}$ solution.

2.5. Detection of PCB77 by PP-AuNPs-Ap/Au Electrode

PCB77, a structurally coplanar compound and one of the most toxic PCB congeners, causes cancer in animals and is a probable human carcinogen. PCB77 is selected as the target compound, and 8 μL of PCB77 solution is added into the 5 mmol L^{-1} $[Fe(CN)_6]^{4-/3-}$ solution for 5 min to ensure sufficient PCB77 binding aptamer. Subsequently, DPV is performed on the PP-AuNP-Ap/Au biosensor in 5 mmol L^{-1} $[Fe(CN)_6]^{4-/3-}$ to detect the response signal of PCB77.

2.6. Safety considerations

PCBs are carcinogenic agents. HMA has a strong amine odor and can cause serious burns and severe irritation. The MSDS information of these chemicals should follow the instruction, and precautions need to be taken for handling them (i.e., wearing gloves, safety glasses and masks).

3. Results and discussion

3.1. Physical characterization of PP and PP-AuNPs

The morphology of the obtained PP are characterized by TEM. Fig. 1 displays representative TEM images of PP and PP-AuNPs. As shown in Fig. 1a, high-quality PP is prepared by the liquid exfoliation method. Fig. 1b is a TEM image of the PP-AuNP nanocomposites and clearly shows the modification of the PP by the nanosized gold nanoparticles, which are dispersed on the PP surface. As shown in Fig. 1b and c, the gold nanoparticles cover 8% of the PP surface after the doping of gold nanoparticles onto PP. The size of the gold nanoparticles is approximately 10–20 nm (Fig. 1c, enlarged Fig. 1b). The structures of PP and of the PP-AuNP nanocomposites are also characterized by SEM. Fig. 2a shows that high-quality PP has been prepared and coated in some areas. As shown in Fig. 2b, the gold nanoparticles cover the PP surface. The SEM and TEM images prove that gold nanoparticles have been dotted on the surface of PP. Fig. S1 illustrates that the elements gold and phosphorus appear in the energy-dispersive X-ray spectroscopy (EDX) curve of the PP-AuNPs.

The stability of the modified PP is also characterized by AFM. As shown in Fig. S2A and B, without the HMA coating, the PP degenerates completely in aqueous solution within 12 h. This result is consistent with previous reports (Kwak et al., 2018). With the HMA coating on the surface, PP maintains its original form in aqueous solution over one month (Fig. S2C and D). The thickness of the HMA coating on the PP is also characterized by AFM. As shown in Fig. S3, the thickness of the HMA coating is approximately 1.4 nm, and a uniform protection layer is formed on the surface of the PP. The PP that can exist stably in aqueous solution could be a promising platform for biosensors.

The structural information of the PP is also characterized by raman spectroscopy and XRD. The raman spectroscopy can provide detailed vibrational and rotational modes of the PP. Fig. S4A shows the structural transformation of the PP and the functionalization PP. The PP shows three peaks at 361 cm^{-1} (the out-of-plane vibrational mode A_g^1), 435 cm^{-1} (the in-plane vibrational mode B_{2g}) and 463 cm^{-1} (the in-plane vibrational mode A_g^2). After coating HMA, these three distinct peaks still exist, indicating that the functionalization PP maintain its original form. As shown in Fig. S4B, XRD pattern of the PP shows the orthorhombic crystal structure along the (040) direction. After coating HMA, the XRD pattern does not change (data not show in Fig. S4B). This confirms that the functionalization PP keeps its original form.

Based on these results, the PP-AuNPs nanocomposite preparation mechanism is illustrated. A weak covalent bond is formed between the amine group and the surface of the gold nanoparticles. The possible mechanism is the nitrogen atoms accepting electrons from the Au and the formation of a weak covalent bond between the amine group and the surface of the gold nanoparticles. This mechanism is consistent with the conclusion from zhou's group and toby's group (Sainsbury et al., 2007; Zhou et al., 2010).

3.2. Monitoring the immobilization of the PP-AuNPs-Ap/Au biosensor

As is well known, the superb materials enhance the performances of the biosensors. The stability of the immobilized material is a basic requirement for a biosensing platform. Even though PP has excellent conductivity (1000 $cm^2/V\,s$), few studies use PP as a biosensing platform due to its easy degradation in aqueous solvent. Now the stable PP has been obtained in our work, the PP shows promise for application as a biosensing platform. In this work, the modification process of the Au electrode is monitored through CV in 5 mmol L^{-1} $[Fe(CN)_6]^{4-/3-}$

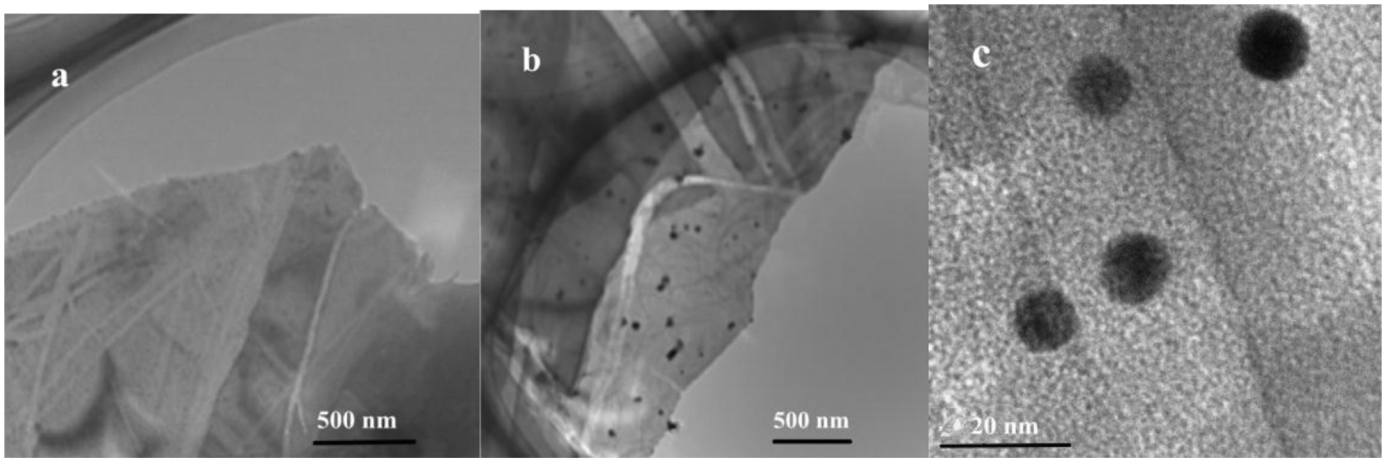

Fig. 1. TEM images of (a) PP and (b) the PP-AuNP nanocomposite and (c) an enlarged image of the PP-AuNP nanocomposite.

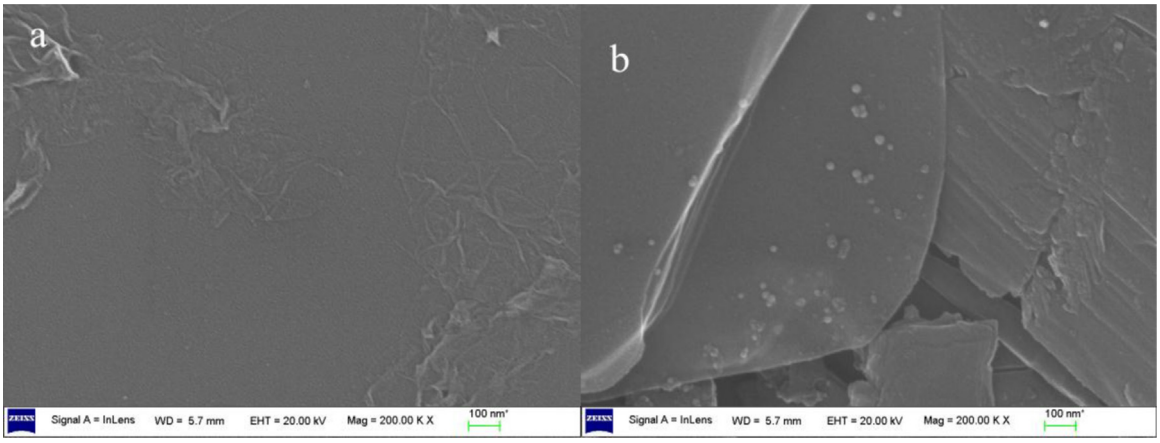

Fig. 2. SEM images of (a) PP and (b) the PP-AuNP nanocomposite.

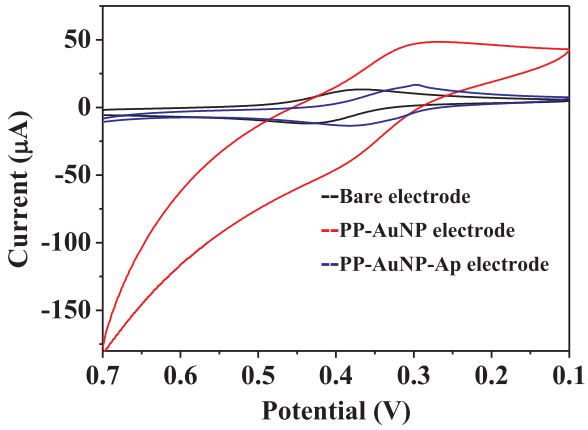

Fig. 3. Cyclic voltammograms of the different Au electrodes in 5 mmol L^{-1} $[Fe(CN)_6]^{3-/4-}$. (a) Bare Au electrode (black line), (b) PP-AuNP/Au electrode (red line) and (c) PP-AuNP-Ap/Au electrode (blue line). (For interpretation of the references to color in this figure legend, the reader is referred to the web version of this article.)

solution. Fig. 3 displays the CV curve of the bare Au electrode, PP-AuNP/Au electrode and PP-AuNP-Ap/Au electrode (curve a, curve b and curve c) in 5 mmol L^{-1} $[Fe(CN)_6]^{4-/3-}$ solution. The peak separation between the cathodic and anodic peaks is 65 mV. It indicates that the electrode redox reaction is a reversible one-electron transfer process and the bare electrode is very clean (Evans, 2008; Grden, 2017). The response signal of the PP-AuNP/Au electrode (curve b) increases significantly in $[Fe(CN)_6]^{4-/3-}$ solution. This is mainly due to the PP-AuNP nanocomposites covering the Au electrode surface. When the aptamer is anchored on the PP-AuNP/Au electrode, the response signal decreases significantly. The reason is that most of the redox signal molecules ($[Fe(CN)_6]^{4-/3-}$) keep a longer distance from the PP-AuNP-Ap/Au electrode surface than from the PP-AuNP/Au electrode surface, and the introducing aptamers have low conductivity. It indicates that the thiol-aptamer is anchored on the PP-AuNP/Au electrode.

3.3. The PP-AuNP-Ap/Au electrode detection of PCB77

PCB77, a structurally coplanar dioxin-like PCB, rendered as definite carcinogen in human by the International Agency for Research on Cancer (Gunawickrama et al., 2008; Su et al., 2015). Due to its bioaccumulation and immunotoxic effects (de Roode et al., 2002; Wang et al., 2010), PCB77 was added in the list of marine monitoring programs in 2006 (Danis et al., 2006). For these reasons, PCB77 is selected as the monitoring chemical molecule. As one of the most sensitive methods, DPV is used for detecting the PCB77 concentration by the PP-AuNP-Ap/Au biosensor. Redox-active ferrocene molecules are used for electrochemical magnification of the response signal. Fig. 4 shows that the response signal of the biosensor is improved with the addition of PCB77. With the addition of PCB77 (from 100 pg L^{-1} to 10 μg L^{-1}), as shown in Fig. 4A, the response signal of the PP-AuNP-Ap/Au biosensor successively increases. This biosensor has a low detection limit (DL) of 33 pg L^{-1} toward PCB77 with a dynamic response range toward PCB77 from 100 pg L^{-1} to 10 μg L^{-1}. The DL of this biosensor (33 pg L^{-1}) significantly surpasses the DLs obtained using previously reported

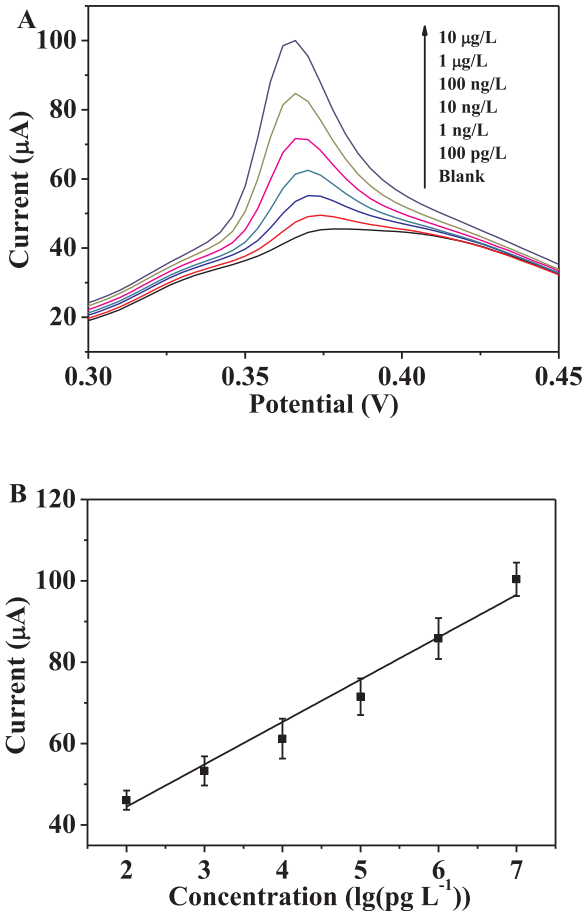

Fig. 4. (A) Differential pulse voltammograms of the PP-AuNP-Ap/Au biosensor at concentrations of PCB77 ranging from 100 pg L^{-1} to 10 μg L^{-1}. Pulse amplitude, 50 mV. (B) The increase in the peak current for different concentrations of PCB77. The standard deviations are all less than 5%.

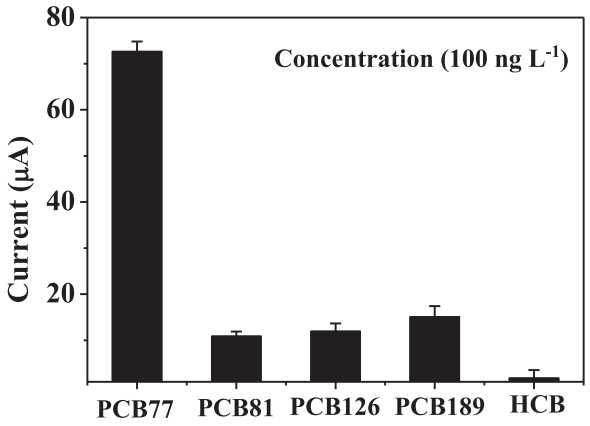

Fig. 5. Screening of four PCBs (3,3′,4,4′-PCB, PCB77; 3,4,4′,5-PCB, PCB81; 3,3′,4,4′,5-PCB, PCB126; 2,3,3′,4,4′,5,5′-PCB, PCB189) and hexachlorobenzene (HCB) using the PP-AuNP-Ap/Au biosensor.

methods (Table S1)(Chen et al., 2016; Fu et al., 2015; Pilehvar et al., 2014). The possible mechanism of the identification of PCB77 by the aptamer is shown in Scheme 1. Before the aptamer binds PCB77, no helix or hairpin structures are formed by the aptamer. The random linear structure of the aptamer keeps the ferrocene (signal molecules) a long distance from the electrode. As a result, there is no response signal before the binding of PCB77. Upon binding PCB77, the aptamer forms a hairpin structure (Xu et al., 2012), which allows the ferrocene to touch the electrode. Then, there is an obvious response signal from the electrode.

Furthermore, the sensitivity and reliability of the Ap/Au biosensor, the AuNP-Ap/Au biosensor and the PP-AuNP-Ap/Au biosensor are systematically tested. Sensitivity is the slope of the calibration curve, i.e., $(R_{ss}-R_{bl})/c$. R_{ss} is the response signal of the biosensor after the addition of standard solutions of the analyte, R_{bl} is the response signal of the background, and c is the analyte concentration (Thevenot et al., 2001). The sensitivities of the Ap/Au biosensor, the AuNP-Ap/Au biosensor and the PP-AuNP-Ap/Au biosensor are 116.6, 147.2 and 391.1 μA cm^{-2}, respectively. The reliability of the biosensor for given samples depends on both selectivity and reproducibility. The selectivity of the biosensor is the ratio of the signal output with the analyte alone to that with the interfering substance alone. The selectivity of the PP-AuNP-Ap/Au biosensor is tested against hexachlorobenzene (HCB) and other coplanar PCBs. Fig. 5 shows the DPV signals of the PP-AuNP-Ap/Au biosensor against 5 types of target analytes (100 ng L^{-1}). Due to the excellent selectivity of the aptamer, the signal of PCB77 shows the most significant change among the tested chemicals. Benzene derivatives (i.e., chlorobenzene, *p*-cresol and phenol) always coexist with PCB77 in the environment. They also have similar physicochemical properties. These chemicals are also screened by the biosensor. There is no signal changes for these benzene derivatives in this study, so these data are not shown in Fig. 5.

The reproducibility is a measure of the scatter of the drift in a series of results obtained over a period of time. It is generally determined for the analyte concentrations within the usable range (Thevenot et al., 2001). Fig. S5 shows the response signals for the determination of PCB77 at 100 ng L^{-1} by the PP-AuNP-Ap/Au biosensor 8 times with a sample testing interval of an hour. The relative standard deviation (RSD) of the 8 testing results by the PP-AuNP-Ap/Au biosensor is under 5%, which indicates that the PP with the protective layer is stable enough to serve as an immobilization platform for the biosensor. It does not degenerate easily in aqueous solution with an output current, and it is not a single-use biosensor. The storage stability is another important characteristic of the PP-AuNP-Ap/Au biosensor. After refrigeration at 4 °C for one week, this biosensor retained over 90% of its initial response signal.

3.4. Monitoring of tap water samples by the PP-AuNP-Ap/Au electrode

In this work, the PP-AuNP-Ap/Au biosensor used for evaluating tap water samples from different areas. The PP-AuNP-Ap/Au biosensor shows that four tap water samples contain PCB77, and their response signals increase by 15%, 24%, 30% and 34%, respectively. As shown in Table S2, the differences in the concentrations obtained by the biosensor and GC-MS are −29.4%, −6.7%, 13.6% and 10.0%, respectively, which indicates that the biosensor detection results are in good agreement with the GC-MS results. These results show that the developed biosensor has potential as an efficient device for the selective detection of PCB77 from environmental samples, although it might not be very precise.

4. Conclusions

The PP is far more air-sensitive and difficult to integrate on electrode. Thus, there have been relatively few air-stability research. The current study develops a simple method for stabilizing PP to overcome its air-sensitive property. After coating HMA, the long-term stability of PP achieves one month, and the coating PP reserves intrinsic properties. The stable PP is used as a biosensing platform, and this PP constructed biosensor exhibits a concentration-dependent response to PCB77 with a low detection limit and high selectivity. Coating PP provides an exciting opportunity to prepare kinds of transistor or biosensor device under humidity. Looking forward to the future, scalable and controllable synthesis method need to develop for commercial application.

Acknowledgments

This work was supported by the National Natural Science Foundation of China (No. 21307161), Projects of Beijing Municipal Science and Technology Project (No. D17110500190000), and the Projects of Beijing Technology and Business University Youth Fund (No. QNJJ2017-06).

Appendix A. Supplementary material

Supplementary data associated with this article can be found in the online version at doi:10.1016/j.bios.2018.10.037.

References

Bui, D.H., Yarmohammadi, M., 2018. Impurity-induced anisotropic semiconductor-semimetal transition in monolayer biased black phosphorus. Phys. Lett. A 382 (28), 1885–1889.

Chen, M., Gan, N., Zhang, H.R., Yan, Z.D., Li, T.H., Chen, Y.J., Xu, Q., Jiang, Q.L., 2016. Electrochemical simultaneous assay of chloramphenicol and PCB72 using magnetic and aptamer-modified quantum dot-encoded dendritic nanotracers for signal amplification. Microchim. Acta 183 (3), 1099–1106.

Danis, B., Cattini, C., Teyssie, J.L., Villeneuve, J.P., Fowler, S.W., Warnau, M., 2006. Coplanar and non-coplanar congener-specificity of PCB bioaccumulation and immunotoxicity in sea stars. Aquat. Toxicol. 79 (2), 105–113.

de Roode, D.F., Vuorinen, P.J., Bosveld, A.T.C., 2002. Effects of furazolidone, PCB77, PCB126, Aroclor 1248, paraquat and p,p '-DDE on transketolase activity in embryonal chicken brain. Toxicology 173 (3), 203–210.

Evans, D.H., 2008. One-electron and two-electron transfers in electrochemistry and homogeneous solution reactions. Chem. Rev. 108 (7), 2113–2144.

Fu, C.C., Wang, Y., Chen, G., Yang, L.Y., Xu, S.P., Xu, W., 2015. Aptamer-based surface-enhanced raman scattering-microfluidic sensor for sensitive and selective polychlorinated biphenyls detection. Anal. Chem. 87 (19), 9555–9558.

Grden, M., 2017. Semi-differential analysis of irreversible voltammetric peaks. J. Solid State Electr. 21 (4), 1045–1058.

Gunawickrama, S.H.N.P., Aarsaether, N., Orbea, A., Cajaraville, M.P., Goksoyr, A., 2008. PCB77 (3,3 ',4,4 '-tetrachlorobiphenyl) co-exposure prolongs CYP1A induction, and sustains oxidative stress in B(a)P-exposed turbot, Scophthalmus maximus, in a long-term study. Aquat. Toxicol. 89 (2), 65–74.

Guo, W.L., Song, H.Z., Yan, S.C., 2018. Stable black phosphorus quantum dots for alkali PH sensor. Opt. Commun. 406, 91–94.

Hu, H.G., Gao, H., Gao, L.L., Li, F., Xu, N., Long, X.F., Hu, Y.P., Jin, J., Ma, J.T., 2018. Covalent functionalization of black phosphorus nanoflakes by carbon free radicals for durable air and water stability. Nanoscale 10 (13), 5834–5839.

Jeong, M.H., Kwak, D.H., Ra, H.S., Lee, A.Y., Lee, J.S., 2018. Realizing long-term stability and thickness control of black phosphorus by ambient thermal treatment. Acs Appl. Mater. Inter 10 (22), 19069–19075.
Jiang, J.W., Park, H.S., 2014a. Mechanical properties of single-layer black phosphorus. J. Phys. D. Appl. Phys. 47 (38), 385304–385306.
Jiang, J.W., Park, H.S., 2014b. Negative poisson's ratio in single-layer black phosphorus. Nat. Commun. 5, 4727–4734.
Kumar, V., Brent, J.R., Shorie, M., Kaur, H., Chadha, G., Thomas, A.G., Lewis, E.A., Rooney, A.P., Nguyen, L., Zhong, X.L., Burke, M.G., Haigh, S.J., Walton, A., McNaughter, P.D., Tedstone, A.A., Savjani, N., Muryn, C.A., O'Brien, P., Ganguli, A.K., Lewis, D.J., Sabherwal, P., 2016. Nanostructured aptamer-functionalized black phosphorus sensing platform for label-free detection of myoglobin, a cardiovascular disease biomarker. Acs Appl. Mater. Inter 8 (35), 22860–22868.
Kwak, D.H., Ra, H.S., Yang, J., Jeong, M.H., Lee, A.Y., Lee, W., Hwang, J.Y., Lee, J.H., Lee, J.S., 2018. Recovery mechanism of degraded black phosphorus field-effect transistors by 1,2-ethanedithiol chemistry and extended device stability. Small 14 (6), 1703194–1703201.
Late, D.J., 2016. Liquid exfoliation of black phosphorus nanosheets and its application as humidity sensor. Micro. Mesopor Mat. 225, 494–503.
Lee, G., Kim, S., Jung, S., Jang, S., Kim, J., 2017. Suspended black phosphorus nanosheet gas sensors. Sens. Actuat B-Chem. 250, 569–573.
Li, L.K., Yu, Y.J., Ye, G.J., Ge, Q.Q., Ou, X.D., Wu, H., Feng, D.L., Chen, X.H., Zhang, Y.B., 2014a. Black phosphorus field-effect transistors. Nat. Nanotechnol. 9 (5), 372–377.
Li, P., Zhang, D.Z., Jiang, C.X., Zong, X.Q., Cao, Y.H., 2017. Ultra-sensitive suspended atomically thin-layered black phosphorus mercury sensors. Biosens. Bioelectron. 98, 68–75.
Li, Y., Yang, S.X., Li, J.B., 2014b. Modulation of the electronic properties of ultrathin black phosphorus by strain and electrical field. J. Phys. Chem. C 118 (41), 23970–23976.
Liu, Y., Wang, Y., Ikram, M., Lv, H., Chang, J., Li, Z., Ma, L., Rehman, A.U., Lu, G., Chen, J., Shi, K., 2018. Facile synthesis of highly dispersed Co3O4 nanoparticles on expanded, thin black phosphorus for a ppb-level NO x gas sensor. ACS Sens. 3 (8), 1576–1583.
Luo, Y., Wu, H., Liu, L., Li, Q., Jiang, K., Fan, S., Li, J., Wang, J., 2018. TiO2-nanocoated black phosphorus electrodes with improved electrochemical performance. ACS Appl. Mater. Interfaces.
Mayorga-Martinez, C.C., Sofer, Z., Pumera, M., 2015. Layered black phosphorus as a selective vapor sensor. Angew. Chem. Int. Ed. 54 (48), 14317–14320.
Miao, J.S., Cai, L., Zhang, S.M., Nah, J., Yeom, J., Wang, C., 2017. Air-stable humidity sensor using few-layer black phosphorus. Acs Appl. Mater. Inter 9 (11), 10019–10026.
Pilehvar, S., Rather, J.A., Dardenne, F., Robbens, J., Blust, R., De Wael, K., 2014. Carbon nanotubes based electrochemical aptasensing platform for the detection of hydroxylated polychlorinated biphenyl in human blood serum. Biosens. Bioelectron. 54, 78–84.
Qiao, J.S., Kong, X.H., Hu, Z.X., Yang, F., Ji, W., 2014. High-mobility transport anisotropy and linear dichroism in few-layer black phosphorus. Nat. Commun. 5, 4475–4482.
Sainsbury, T., Ikuno, T., Okawa, D., Pacile, D., Frechet, J.M.J., Zettl, A., 2007. Self-assembly of gold nanoparticles at the surface of amine- and thiol-functionalized boron nitride nanotubes. J. Phys. Chem. C 111 (35), 12992–12999.
Su, K., Lv, X.F., Song, H., Luo, X.S., Chen, C., 2015. PCB77 inducing renal tubular cell apoptosis. Ultrastruct. Pathol. 39 (3), 192–197.
Tan, W.C., Cai, Y., Ng, R.J., Huang, L., Feng, X., Zhang, G., Zhang, Y.W., Nijhuis, C.A., Liu, X., Ang, K.W., 2017. Few-layer black phosphorus carbide field-effect transistor via carbon doping. Adv. Mater. 29 (24).
Thevenot, D.R., Toth, K., Durst, R.A., Wilson, G.S., 2001. Electrochemical biosensors: recommended definitions and classification. Biosens. Bioelectron. 16 (1–2), 121–131.
Wan, B.S., Zhou, Q.H., Zhang, J.Y., Wang, Y., Yang, B.C., Lv, W.M., Zhang, B.S., Zeng, Z.M., Chen, Q., Wang, J.L., Wang, W.H., Wen, F.S., Xiang, J.Y., Xu, B., Zhao, Z.S., Tian, Y.J., Liu, Z.Y., 2018. Enhanced stability of black phosphorus field-effect transistors via hydrogen treatment. Adv. Electron Mater. 4 (2), 1700455–1700462.
Wang, J., Lv, X.W., Du, Y.G., 2010. Inflammatory response and insulin signaling alteration induced by PCB77. J. Environ. Sci.-China 22 (7), 1086–1090.
Wu, L., Lu, X., Zhang, H., Chen, J., 2012. Amino acid ionic liquid modified mesoporous carbon: a tailor-made nanostructure biosensing platform. Chemsuschem 5 (10), 1918–1925.
Xing, C.Y., Jing, G.H., Liang, X., Qiu, M., Li, Z.J., Cao, R., Li, X.J., Fan, D.Y., Zhang, H., 2017. Graphene oxide/black phosphorus nanoflake aerogels with robust thermostability and significantly enhanced photothermal properties in air. Nanoscale 9 (24), 8096–8101.
Xu, S.M., Yuan, H., Chen, S.P., Xu, A., Wang, J., Wu, L.J., 2012. Selection of DNA aptamers against polychlorinated biphenyls as potential biorecognition elements for environmental analysis. Anal. Biochem. 423 (2), 195–201.
Zhang, J.N., Chen, S., Ma, Y., Wang, D.Y., Zhang, J., Wang, Y.D., Li, W.J., Yu, Z.Q., Zhang, H., Yin, F., Li, Z.G., 2018. Organosilicon modification to enhance the stability of black phosphorus nanosheets under ambient conditions. J. Mater. Chem. B 6 (24), 4065–4070.
Zhao, Y., Zhang, Y.H., Zhuge, Z., Tang, Y.H., Tao, J.W., Chen, Y., 2018. Synthesis of a poly-L-lysine/black phosphorus hybrid for biosensors. Anal. Chem. 90 (5), 3149–3155.
Zhou, J.C., Wang, X.H., Xue, M., Xu, Z., Hamasaki, T., Yang, Y., Wang, K., Dunn, B., 2010. Characterization of gold nanoparticle binding to microtubule filaments. Mat. Sci. Eng. C.-Mater. 30 (1), 20–26.